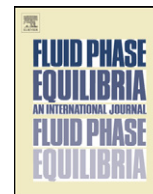




Contents lists available at SciVerse ScienceDirect

Fluid Phase Equilibria

journal homepage: www.elsevier.com/locate/fluid

On the prediction of transport properties of monomethylamine, dimethylamine, dimethylether and hydrogen chloride by molecular simulation

G. Guevara-Carrion^a, J. Vrabec^{b,*}, H. Hasse^a^a Laboratory for Engineering Thermodynamics, Technical University of Kaiserslautern, Erwin-Schrödinger-Straße 44, 67663 Kaiserslautern, Germany^b Thermodynamics and Energy Technology, University of Paderborn, Warburger Straße 100, 33098 Paderborn, Germany

ARTICLE INFO

Article history:

Received 19 September 2011

Received in revised form 7 November 2011

Accepted 5 December 2011

Available online 13 December 2011

Keywords:

Green–Kubo

Reverse non-equilibrium molecular dynamics

Diffusion coefficient

Shear viscosity

Thermal conductivity

ABSTRACT

Molecular modeling and simulation has emerged in recent years as a powerful engineering tool for the prediction of thermodynamic properties of fluids. In this work, transport properties of monomethylamine, dimethylamine, dimethylether and hydrogen chloride are predicted by molecular simulation, employing rigid, non-polarizable molecular models that were developed without using any transport property information. Equilibrium molecular dynamics as well as non-equilibrium molecular dynamics are used to predict self-diffusion coefficient, shear viscosity and thermal conductivity of the studied liquids for a wide range of thermodynamic conditions. In most cases, the reported predictions deviate on average by less than 10% from the available experimental data.

© 2011 Elsevier B.V. All rights reserved.

1. Introduction

In recent years, the need for transport data has increased in the chemical industry. Among others, this is due to the growing use of rate-based methods for process modeling. Traditionally, thermodynamic properties are obtained from experiments, however, despite the extensive effort devoted to their measurement, the data availability is still surprisingly low and the data sets are in many cases contradictory. This is associated with the significant effort to measure thermophysical properties, particularly at very high temperatures and pressures [1], or to deal experimentally with substances that are toxic or explosive. Compared to static properties like vapor–liquid equilibria, transport data are very scarce. Because traditional phenomenological models for transport properties are little reliable in the liquid state, molecular simulation has emerged as an alternative engineering tool for predictive applications.

The aim of this work is to demonstrate the capability of molecular modeling and simulation to predict the technically most relevant transport properties, i.e. self-diffusion coefficient, shear viscosity and thermal conductivity, of monomethylamine (MMA, $\text{CH}_3\text{-NH}_2$), dimethylamine (DMA, $(\text{CH}_3)_2\text{-NH}$), dimethylether (DME, $(\text{CH}_3)_2\text{-O}$) and hydrogen chloride (HCl). As in previous work

of our group, rigid, non-polarizable molecular models were used. This model class is suitable to predict structural and thermodynamic properties of hydrogen bonding fluids with a good accuracy, e.g. water, methanol, ethanol, ammonia and some binary mixtures thereof [2–4]. Equilibrium molecular dynamics (EMD) simulation together with the Green–Kubo formalism was used to determine the self-diffusion coefficient and the shear viscosity. The shear viscosity and the thermal conductivity were calculated via the reverse non-equilibrium molecular dynamics (NEMD) algorithm by Müller-Plathe [5]. These transport properties were predicted in the liquid state for a wide range of thermodynamic conditions and a comparison between EMD and NEMD results is given for the shear viscosity.

The studied fluids have important industrial applications. The weakly hydrogen bonding amines MMA and DMA are widely used as intermediates in chemical synthesis, e.g. in the production of solvents, pesticides, pharmaceuticals, dyes or surfactants [6,7]. DME is largely used as a substitute for chlorofluorocarbons, i.e. as an aerosol propellant, refrigerant or petroleum gas [8–10]. It is also used as feedstock for the production of higher value chemicals, e.g. acetic acid or formaldehyde [11]. HCl is a very hazardous fluid that is widely used in the chemical, pharmaceutical, oil and food industry [12], e.g. as an intermediate or catalyst in the production of higher value chemicals [13]. The success of molecular simulation to predict thermodynamic properties is primarily determined by the force field that describes the molecular interactions. Many of the molecular models from the literature for MMA and DMA

* Corresponding author. Tel.: +49 0 5251 60 2421; fax: +49 0 5251 60 3522.

E-mail addresses: jadran.vrabec@uni-paderborn.de, jadran.vrabec@upb.de (J. Vrabec).

are based on transferable force fields developed for biological systems, e.g. OPLS-AA [14], CFF [15] or CHARMM [7], which usually include Lennard–Jones (LJ) sites, point charges as well as internal degrees of freedom, i.e. bond stretching, angle and dihedral bending. Other molecular models are based on transferable force fields that were developed for chemical engineering applications, e.g. the anisotropic united atom force field (AUA) [16], the TraPPE-EH force field [17] or the discontinuous force field SPEAD [18]. They were primarily employed for studying the fluid structure [19] and thermodynamic properties like free energy of hydration [14] or vapor–liquid equilibria [17,18]. However, only a few models were assessed with respect to their capability to predict transport properties. Kosztolányi et al. [20] and Kusalik et al. [21] predicted the self-diffusion coefficient of MMA at 250 K using the rigid model by Impey et al. [22]. Bauer and Patel [7] also predicted the self-diffusion coefficient of MMA at 266.8 K based on their polarizable model. Recently, Feng et al. [23] predicted the self-diffusion coefficient of MMA for different thermodynamic conditions based on a modification of the OPLS-AA model [14]. To our knowledge, the self-diffusion coefficient of DMA as well as the shear viscosity and thermal conductivity of both amines were not studied by molecular simulation prior to this work.

A variety of molecular models for DME can be found in the literature, e.g. flexible models based on transferable [24–26], discontinuous [27] or polarizable [28] force fields as well as rigid models [29–31]. However, to our knowledge, none of them was employed to predict the transport properties of DME by molecular simulation.

HCl is the smallest molecule considered in this work and has therefore been subject to numerous molecular simulation and quantum mechanical studies in the last 30 years. For HCl, there are several molecular models of different complexity in the literature, e.g. [32–41]. Some of them were used to predict the self-diffusion coefficient [32,33,36,37,41] and the shear viscosity [42] by molecular simulation. The thermal conductivity was not studied prior to this work.

The molecular models employed here for MMA [43], DMA [43], DME [44] and HCl [13] were developed in preceding work of our group. These rigid, united-atom models were optimized to experimental data on vapor pressure and saturated liquid density only. No data on transport properties were taken into account during model parameterization so that all respective results are strictly predictive.

The outline of the present work is as follows: first, the employed molecular models and the simulation techniques are briefly described. Second, the predictions for self-diffusion

coefficient, shear viscosity and thermal conductivity of the studied liquids are presented and compared to experimental data and correlations thereof as well as to other simulation results from the literature. Finally, conclusions are drawn. The simulation details are summarized in Appendix B.

2. Molecular models

Throughout this work, rigid, non-polarizable molecular models of united-atom type from earlier work of our group were used. The models account for the intermolecular interactions by one or more LJ sites and superimposed point charges or point dipoles. Thus, the total intermolecular interaction energy u_{ij} between two molecules i and j can be written as

$$u_{ij}(r_{ijab}) = \sum_{a=1}^{S_i^L} \sum_{b=1}^{S_j^L} 4\epsilon_{ijab} \left[\left(\frac{\sigma_{ijab}}{r_{ijab}} \right)^{12} - \left(\frac{\sigma_{ijab}}{r_{ijab}} \right)^6 \right] + \sum_{c=1}^{S_i^e} \sum_{d=1}^{S_j^e} \frac{q_{ic}q_{jd}}{4\pi\epsilon_0 r_{ijcd}} + \frac{\mu_{ic}\mu_{jd}}{4\pi\epsilon_0 r_{ijcd}^3} \cdot f(\omega_i, \omega_j), \quad (1)$$

where r_{ijab} , ϵ_{ijab} and σ_{ijab} are the distance, the LJ energy parameter and the LJ size parameter, respectively, for the pair-wise interaction between LJ site a on molecule i and LJ site b on molecule j . The permittivity of the vacuum is ϵ_0 , whereas q_{ic} and μ_{ic} denote the point charge magnitude and the dipole moment of the electrostatic interaction site c on molecule i . The expression $f(\omega_i, \omega_j)$ stands for the dependency of the dipole interaction on the orientations ω_i and ω_j of the molecules i and j [45]. The pure substance model parameters were taken from [13,43,44] and are summarized in Table 1. The interactions between unlike LJ sites of different type were defined by the standard Lorentz–Berthelot combining rules

$$\sigma_{ab} = \frac{\sigma_{aa} + \sigma_{bb}}{2}, \quad (2)$$

and

$$\epsilon_{ab} = \sqrt{\epsilon_{aa}\epsilon_{bb}}. \quad (3)$$

3. Methodology

3.1. Equilibrium molecular dynamics

Transport properties can be determined from the time evolution of the autocorrelation function of a particular microscopic flux in

Table 1

Lennard–Jones and electrostatic parameters of the molecular models employed in this work. The orientation of the dipole moment is defined in standard Euler angles, where φ is the azimuthal angle with respect to the x – z plane and θ is the inclination angle with respect to the z axis. The spatial position of the sites can be found in the original publications [13,43,44].

Interaction sites	σ (Å)	ϵ/k_B (K)	θ (°)	φ (°)	μ (D)	q (e)
Monomethylamine						
CH ₃	3.6072	120.150	–	–	–	+1.95250
NH ₂	3.3151	141.147	–	–	–	–0.88653
H	–	–	–	–	–	+0.34564
Dimethylamine						
CH ₃	3.6072	120.150	–	–	–	+0.03774
NH	3.4800	72.856	–	–	–	–0.45959
H	–	–	–	–	–	+0.38411
Dimethylether						
O	2.727	89.570	–	–	–	–
CH ₃	3.6072	120.150	–	–	–	–
Dipole	–	–	180	0	1.7040	–
Hydrogen chloride						
HCl	3.520	179.00	–	–	–	–
H	–	–	–	–	–	+0.438
Cl	–	–	–	–	–	–0.438

a system in equilibrium using the Green–Kubo formalism [46,47]. This method relates a transport coefficient to the time integral of an autocorrelation function of a particular microscopic flux. It was used here to calculate the self-diffusion coefficient and the shear viscosity.

The general Green–Kubo expression for a transport coefficient γ is given by

$$\gamma = \frac{1}{G} \int_0^\infty dt \langle \dot{\mathbf{A}}(t) \cdot \dot{\mathbf{A}}(0) \rangle, \quad (4)$$

where G is a property dependent prefactor, \mathbf{A} is the related perturbation and $\dot{\mathbf{A}}$ its time derivative. $\langle \dots \rangle$ denotes the ensemble average.

In the case of the self-diffusion coefficient, $\mathbf{A}(t)$ stands for the position vector of a molecule k at some time t , i.e. $\mathbf{r}_k(t)$, and $\dot{\mathbf{A}}_k(t)$ is the center of mass velocity vector, i.e. $\mathbf{v}_k(t)$. Thus, the self-diffusion coefficient D_i is related to the individual molecule velocity autocorrelation function as follows

$$D_i = \frac{1}{3N} \int_0^\infty dt \langle \mathbf{v}_k(t) \cdot \mathbf{v}_k(0) \rangle. \quad (5)$$

Eq. (5) is an average over all N molecules in the ensemble, since all contribute to the self-diffusion coefficient.

The shear viscosity η is associated with the time autocorrelation function of the off-diagonal elements of the stress tensor J_p^{xy} [48]

$$\eta = \frac{1}{Vk_B T} \int_0^\infty dt \langle J_p^{xy}(t) \cdot J_p^{xy}(0) \rangle, \quad (6)$$

where V stands for the molar volume, k_B is the Boltzmann constant and T denotes the temperature. Averaging over all three independent elements of the stress tensor, i.e. J_p^{xy} , J_p^{xz} and J_p^{yz} , improves the statistics of the simulation. The component J_p^{xy} of the microscopic stress tensor \mathbf{J}_p is given by [49]

$$J_p^{xy} = \sum_{i=1}^N m v_i^x v_i^y - \frac{1}{2} \sum_{i=1}^N \sum_{j \neq i} \sum_{a=1}^{S_i} \sum_{b=1}^{S_j} r_{ij}^x \frac{\partial u_{ijab}}{\partial r_{ij}^y}. \quad (7)$$

Here, the lower indices a and b count all interaction sites $S_i = S_i^f + S_i^e$, while the upper indices x and y denote the spatial vector components of the velocity v_i^x and the distance r_{ij}^x .

3.2. Non-equilibrium molecular dynamics

Instead of using the Green–Kubo or Einstein EMD formulations, transport properties can be calculated via non-equilibrium molecular dynamics (NEMD). NEMD methods involve an artificially imposed external field that drives the system out of the equilibrium. Similar to the experiment, the long-time response to this perturbation is measured to determine transport properties. NEMD methods are favored when the signal-to-noise ratio is high at long times, therefore reverse NEMD [5,50,51] was used throughout this work to calculate the thermal conductivity, but also to obtain some shear viscosity data.

To determine the thermal conductivity λ , a heat flux is imposed onto a molecular system, e.g. in the z direction, and the resulting temperature gradient is measured. For this purpose, the simulation volume is divided perpendicular to the z direction into M slabs of identical thickness L_z/M , where L_z is the length of the simulation volume in the z direction. The slab at $z=0$ is defined as the “cold slab” and the one at $z=L_z/2$ as the “hot slab”. In order to create a heat flux, the velocity of the molecule with the highest kinetic energy in the cold slab v_l and the velocity of the molecule with the lowest kinetic energy in the hot slab v_h are interchanged. This mechanism enforces a kinetic energy transfer from the cold slab to the hot slab

that leads to a temperature gradient. In the steady state, this energy transfer is balanced by the heat flux in the opposite direction. The energy flux is given by [5]

$$\langle J \rangle_t = \frac{1}{2At} \sum_{\text{transfers}} \frac{m}{2} (v_h^2 - v_l^2), \quad (8)$$

where A is the cross sectional area in x and y direction and t is the simulation time. The thermal gradient ∇T_z is obtained from a linear fit of the temperature profile resulting from the simulation. In the steady state, the thermal conductivity is thus given by

$$\lambda = -\frac{\langle J \rangle_t}{\nabla T_z}. \quad (9)$$

The shear viscosity η can be calculated via reverse NEMD by measuring the resulting shear rate when a flux of transverse linear momentum is imposed onto the molecular system [51]. The simulation volume is again divided into slabs perpendicular to the z direction. The molecules in the “forward slab” at $z=0$ are propelled in the $+x$ direction, while those in the “backward slab” at $z=L_z/2$ are propelled in the $-x$ direction. This is done by interchanging the momentum component in the x direction $p_x = m \cdot v_x$. The molecule with the largest absolute value of p_x in the $-x$ direction of the forward slab interchanges its momentum with the molecule having the largest absolute value of p_x in the $+x$ direction of the backward slab [51]. The system responds to the momentum transfer by momentum flow in the opposite direction via friction [51]. In the steady state, the imposed momentum flux is balanced by the friction flux in the fluid. The momentum flux is given by [51]

$$\langle J_{p_x} \rangle_t = \frac{1}{2At} \sum_{\text{transfers}} m (v_{x,1} - v_{x,2}). \quad (10)$$

The shear rate is obtained from the gradient of the mean velocity in the x direction of each slab with respect to the z direction. In the steady state, the shear viscosity is thus given by [50]

$$\eta = -\langle J_{p_x} \rangle_t \frac{\partial v_x}{\partial z}. \quad (11)$$

4. Simulation results

The thermodynamic conditions studied in this work were generally chosen according to the availability of experimental data or correlations thereof in the literature which were used for direct comparison with the simulation results. Data for previously unexplored conditions were predicted as well, e.g. for DMA at high pressures.

4.1. Monomethylamine

4.1.1. Self-diffusion coefficient

The pressure dependence of the self-diffusion coefficient of liquid MMA was predicted at 10, 50, 100, 150 and 200 MPa in the temperature range from 203 to 423 K. Fig. 1 shows, exemplarily, the temperature dependence of the self-diffusion coefficient at selected pressures, i.e. 10, 100 and 200 MPa, in comparison to experimental data by Chen et al. [52]. The full numerical simulation results are listed in Table 1 of the Supplementary material. In general, the present results are in very good agreement with the experimental data, the mean deviation is approximately 6% for the whole range of studied conditions. The accuracy of the predicted self-diffusion coefficient is similar to that of the data published by Feng et al. [23] who used a more complex flexible model [14]. A graphical comparison between the present work and the results by Feng et al. [23] at 50 MPa is shown in Fig. 1 of the Supplementary material.

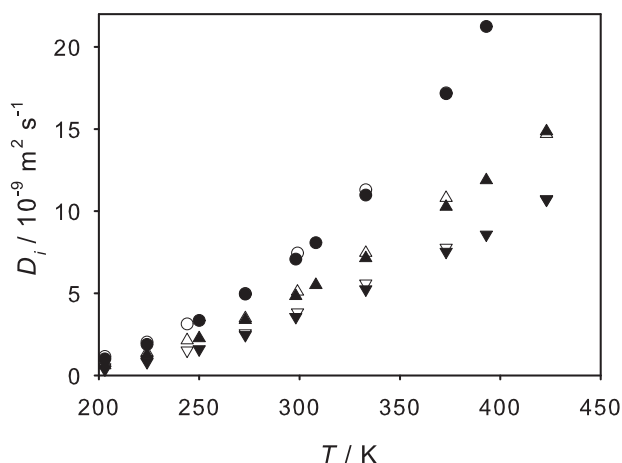


Fig. 1. Temperature dependence of the self-diffusion coefficient of liquid monomethylamine. Present EMD simulation results at 10 (●), 100 (▲) and 200 MPa (▼) are compared to experimental data [52] (open symbols). The error bars are within symbol size.

The self-diffusion coefficient of saturated liquid MMA was predicted at temperatures between 203 and 373 K, the numerical results are given in Table 2 of the Supplementary material. To our knowledge, there are no experimental data in the literature for the self-diffusion coefficient of MMA under these conditions. However, due to the high accuracy shown for liquid MMA in the homogeneous region at high pressures, these results can be expected to match the true fluid behavior.

Both Kosztolányi et al. [20] and Kusalik et al. [21] calculated the self-diffusion coefficient of MMA at 250 K and atmospheric pressure based on the model by Impey et al. [22]. They reported self-diffusion coefficients of 4.93 and $4.31 \times 10^{-9} \text{ m}^2 \text{ s}^{-1}$, respectively. Bauer and Patel [7] reported a self-diffusion coefficient of $3.89 \times 10^{-9} \text{ m}^2 \text{ s}^{-1}$ at 266.8 K and 0.1 MPa using their polarizable model. Curiously, all these authors [7,20,21] compared their simulation results to one experimental value of $5.10 \times 10^{-9} \text{ m}^2 \text{ s}^{-1}$ apparently by Chen et al. [52]. However, Chen et al. [52] only presented experimental results for MMA at pressures of 10 MPa or higher and none of their values near 250 K corresponds to the mentioned experimental self-diffusion coefficient. In the present work, the self-diffusion coefficient at 250 K and 0.1 MPa was calculated to be $3.49 \times 10^{-9} \text{ m}^2 \text{ s}^{-1}$.

4.1.2. Shear viscosity

Fig. 2 shows the shear viscosity of saturated liquid MMA at temperatures between 203 and 373 K compared to experimental data [53–55] and a correlation thereof [56]. The numerical results are given in Table 2 of the Supplementary material. It can be seen that the simulations well predict the temperature dependence of the shear viscosity for the studied temperatures, the average deviation from the correlation is 12.5%. However, the deviation from experimental data is smaller. The lower values of the shear viscosity from simulation with respect to the correlation for temperatures >300 K are in better agreement with the experimental data [53–55]. The statistical uncertainty of the present results is around 12%, being higher for low temperatures due to the elevated density of MMA under these conditions.

The shear viscosity of liquid MMA was predicted here also at high pressures, i.e. 10, 50, 100, 150 and 200 MPa, however, experimental data for comparison are available only at 10 MPa [53]. The agreement between the two data sets is very good, cf. Fig. 3. The average deviation is only 2.8%.

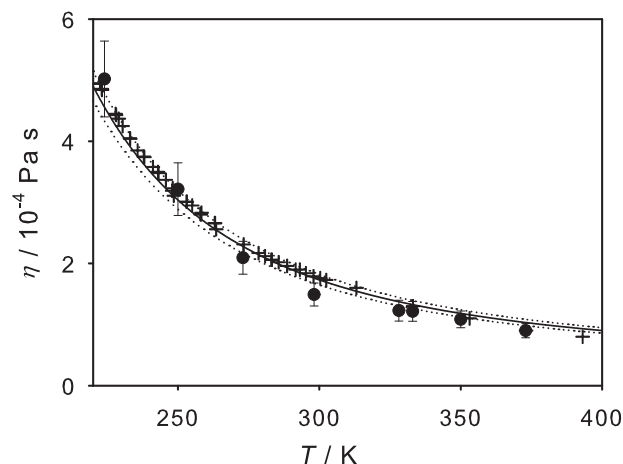


Fig. 2. Temperature dependence of the shear viscosity of saturated liquid monomethylamine. Present EMD simulation results (●) are compared to experimental data [53–55] (+) and to a correlation thereof [56] (-). The dotted lines indicate the uncertainty of the correlation as specified in [56].

4.1.3. Thermal conductivity

Present predictions of the thermal conductivity of saturated liquid MMA at temperatures between 203 and 373 K are compared to experimental data [57,58] and a correlation thereof [56] in Fig. 4. Furthermore, the thermal conductivity was predicted for liquid states in the homogeneous region at 2, 5, 10, 25 and 50 MPa in the temperature range from 293 to 393 K. Fig. 5 shows, exemplary, the present values at 10 and 50 MPa together with experimental data [59]. The numerical results are given in Tables 2 and 3 of the Supplementary material. The thermal conductivity of the saturated liquid from simulation deviates on average by 8% from the correlation, however, the simulation values show a stronger dependence on the temperature than the correlation [56], which has an error margin of 10%. On the other hand, the two available experimental data sets [57,58] are contradictory, cf. Fig. 4. The present results at high pressures are in excellent agreement with the experimental data by Fedosov [59] over the entire range of studied conditions, the average deviation is only 2.2%. Here, the temperature dependence of the thermal conductivity is well predicted by simulation, cf. Fig. 5. Accordingly, the present results suggest possible inaccuracies on the correlation of experimental data by DIPPR [56] for the saturated liquid. This finding is supported by the more pronounced slope of the

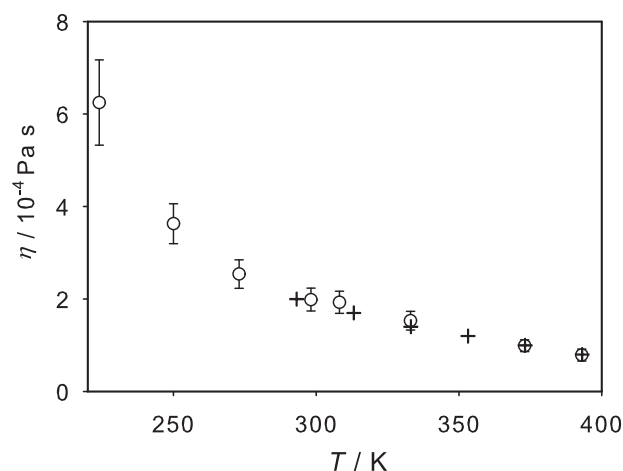


Fig. 3. Temperature dependence of the shear viscosity of liquid monomethylamine. Present EMD simulation results at 10 MPa (○) are compared to experimental data [53] (+).

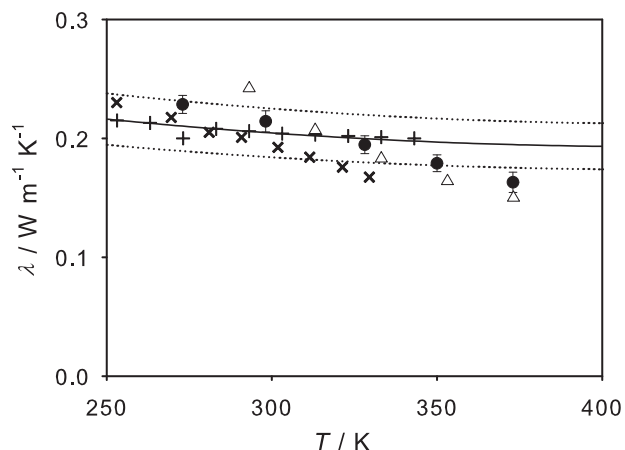


Fig. 4. Temperature dependence of the shear viscosity of saturated liquid monomethylamine. Present EMD simulation results (●) are compared to experimental data by Gallant [58] (×) and by Engineering Sciences Data Unit [57] (+) as well as to a correlation thereof [56] (–). The dotted lines indicate the uncertainty of the correlation as specified in [56]. The experimental data for the homogeneous liquid at 5 MPa [59] (Δ) are also shown.

thermal conductivity dependence on temperature from experiment at 5 MPa, cf. Fig. 4. However, further experimental data or simulations are required for a decisive conclusion.

4.2. Dimethylamine

4.2.1. Self-diffusion coefficient

The self-diffusion coefficient of liquid DMA was predicted along the saturated liquid line and for homogeneous liquid states at 50, 100, 150 and 200 MPa in the temperature range between 203 and 423 K. The numerical results are given in Tables 4 and 5 of the Supplementary material. To our knowledge, the self-diffusion coefficient of DMA has not been determined before neither experimentally nor by molecular simulation. Hence, the simulation results of this work are compared to the self-diffusion coefficient of the amines MMA and trimethylamine (TMA) under the same conditions. Fig. 6 shows this comparison for the three fluids at 50 MPa. Particularly at high temperatures, the self-diffusion coefficient of DMA is higher than that of TMA, but lower than that of MMA, which is expected due to the molecular weight of DMA. This behavior is less pronounced at low temperatures, where the differences between the self-diffusion coefficient of MMA and DMA

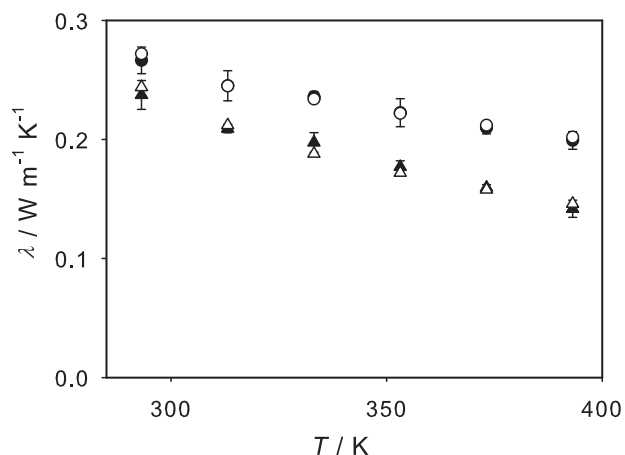


Fig. 5. Temperature dependence of the thermal conductivity of liquid monomethylamine. Present reverse-NEMD simulation results at 10 (●) and 50 MPa (▲) are compared to experimental data [59] (open symbols).

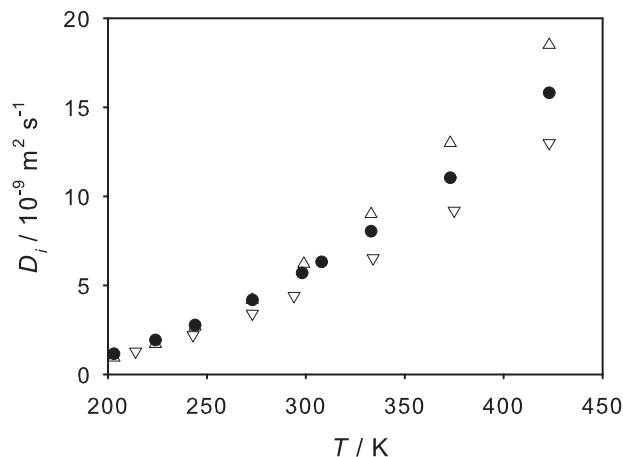


Fig. 6. Temperature dependence of the self-diffusion coefficient of liquid amines at 50 MPa. Present EMD simulation results for dimethylamine (●) are compared to experimental data [52] for monomethylamine (Δ) and trimethylamine (▽) [52]. The error bars are within symbol size.

are smaller, which can be attributed to the presence of hydrogen bonding in MMA and DMA.

4.2.2. Shear viscosity

The predicted shear viscosity of saturated liquid DMA is shown in Fig. 7 in comparison to experimental data [60,61] and a correlation thereof [56]. As can be seen, the present simulation results accurately cover the temperature dependence of the shear viscosity, the mean deviation to the correlation is approximately 7%. The numerical results are given in Table 4 of the Supplementary material. Analogously to MMA, the shear viscosity of liquid DMA was also predicted at high pressures, i.e. 50, 100, 150 and 200 MPa. However, no experimental data are available for validation.

4.2.3. Thermal conductivity

The thermal conductivity of liquid DMA was calculated along the saturated liquid line between 224 and 333 K. Fig. 8 shows the simulation results in comparison to experimental data [57,58] and a correlation thereof [56]. As can be seen, the experimental data sets are contradictory. On the other hand, the present simulation results accurately predict the temperature dependence of the thermal conductivity given by the DIPPR correlation [56] based on the experimental data reported by the Engineering Sciences Data

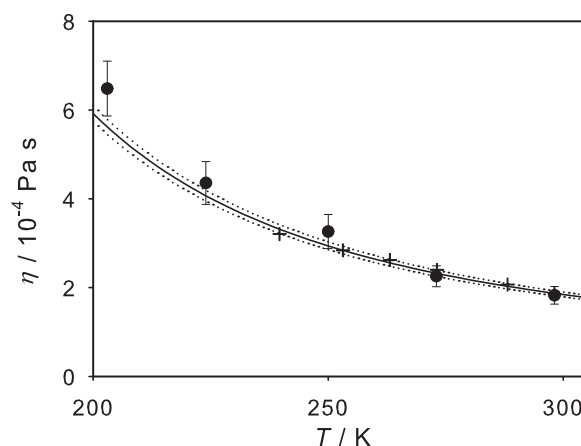


Fig. 7. Temperature dependence of the shear viscosity of saturated liquid dimethylamine. Present EMD simulation results (●) are compared to experimental data [60,61] (+) and to a correlation thereof [56] (–). The dotted lines indicate the uncertainty of the correlation as specified in [56].

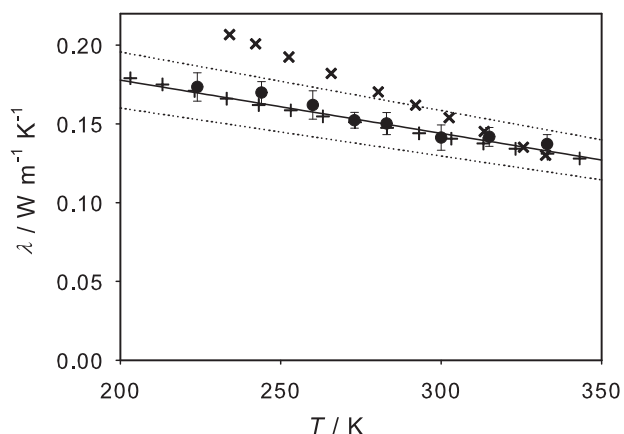


Fig. 8. Temperature dependence of the thermal conductivity of saturated liquid dimethylamine. Present reverse-NEMD simulation results (●) are compared to experimental data by Gallant [58] (×) and by Engineering Sciences Data Unit [57] (+) as well as to a correlation thereof [56] (–). The dotted lines indicate the uncertainty of the correlation as specified in [56].

Unit [57]. They match throughout within their statistical error, cf. Fig. 8. The average deviation between the two data sets is merely 2.2%. Therefore, the present results suggest that the experimental thermal conductivity data reported by Gallant [58] could be inaccurate. However, further simulation or experimental data are required for a conclusive determination.

4.3. Dimethylether

4.3.1. Self-diffusion coefficient

Fig. 9 shows the present simulation results for the temperature dependence of the self-diffusion coefficient of liquid DME at 50, 100 and 200 MPa in comparison to experimental data [62]. The self-diffusion coefficient of DME was also predicted at 150 MPa, which is not shown graphically. All numerical results are given in Table 6 of the Supplementary material. As can be seen in Fig. 9, all predicted data correctly reproduce the temperature dependence of the self-diffusion coefficient and are in good agreement with the experimental data (6% average deviation). However, it can be noticed for temperatures >360 K that there is a tendency to underestimate the self-diffusion coefficient.

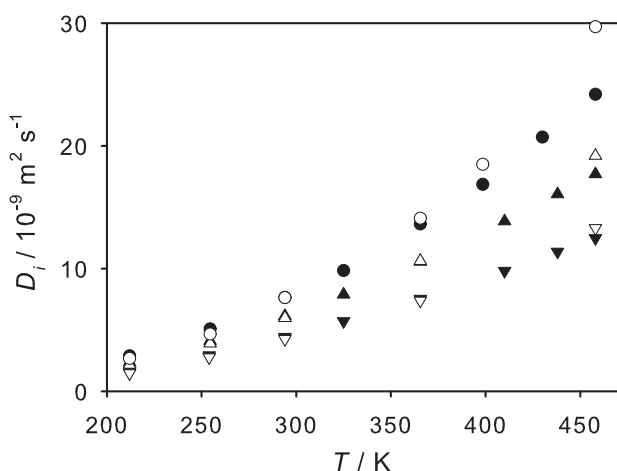


Fig. 9. Temperature dependence of the self-diffusion coefficient of liquid dimethylether. Present EMD simulation results at 50 (●), 100 (▲) and 200 MPa (▼) are compared to experimental data [62] (open symbols). The error bars are within symbol size.

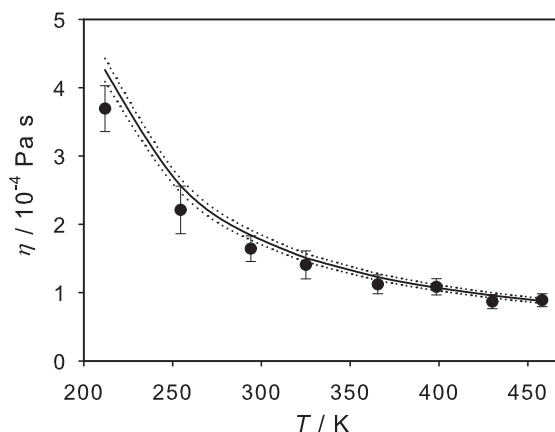


Fig. 10. Temperature dependence of the shear viscosity of liquid dimethylether. Present EMD simulation results at 50 MPa (●) are compared to a correlation based on the estimation method by Huber et al. [63] (–). The dotted lines indicate the uncertainty of the correlation as specified in [63].

4.3.2. Shear viscosity

The shear viscosity of liquid DME was predicted at 50, 100, 150 and 200 MPa in the temperature range between 212 and 458 K. However, only a correlation based on an estimation method at 50 MPa is available in the literature [63]. Thus, only the simulation results at 50 MPa were compared to literature values, cf. Fig. 10. At this pressure, the simulation results agree well with the correlation, the predicted shear viscosity deviates on average by 8% from the correlation. It can be noticed for temperatures <300 K that the simulations tend to underestimate the shear viscosity. The simulation results have a mean statistical uncertainty of around 12%, which is higher at low temperatures due to the high density of the fluid.

4.4. Hydrogen chloride

4.4.1. Self-diffusion coefficient

Fig. 11 shows the present simulation results for the self-diffusion coefficient of saturated liquid HCl between 175 and 310 K in comparison to the available experimental data [64,65] and to simulation results by Powles et al. [32], Murad et al. [37] and Yogi [40]. Numerical data are given in Table 7 of the Supplementary material. As can

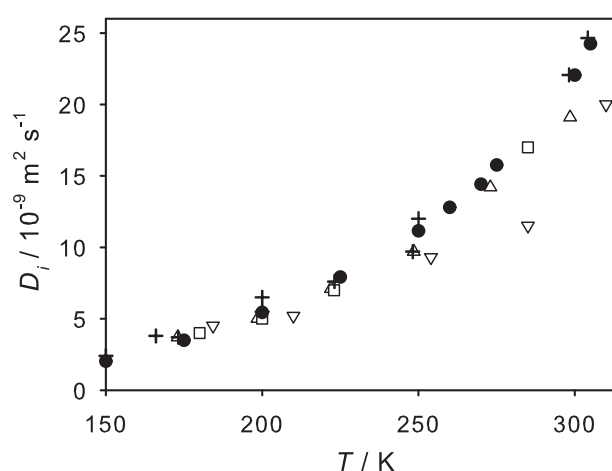


Fig. 11. Temperature dependence of the self-diffusion coefficient of saturated liquid hydrogen chloride. Present EMD simulation results (●) together with the simulation results by Murad et al. [37] (□), by Yogi [40] (△) and by Powles et al. [32] (▽) are compared to experimental data [64,65] (+).

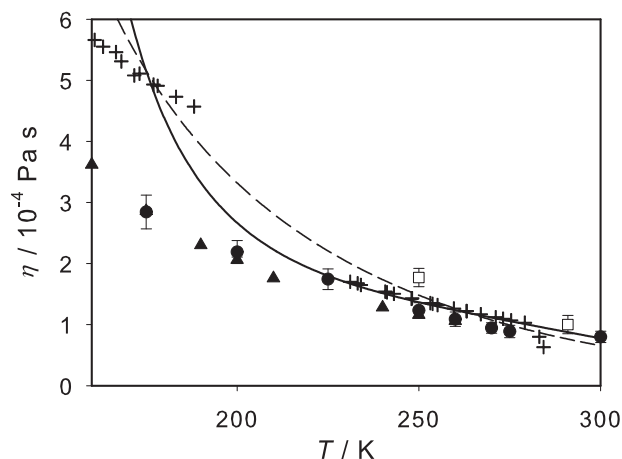


Fig. 12. Temperature dependence of the shear viscosity of saturated liquid hydrogen chloride. Present EMD (●) and reverse-NEMD simulation results (▲) and the simulation results by Kielpinski et al. [42] (□) are compared to experimental data [66–68] (+) as well as to correlations thereof by DIPPR [56] (–) and by Yaws [69] (––).

be seen in Fig. 11, the agreement between simulation and experimental data reported by O'Reilly [64] and Krynicki et al. [65] is very good. The simulation works by Murad et al. [37] and Yogi [40] also reported a good agreement of the predicted self-diffusion coefficient with experimental data using a rigid rotor model [40] and a polarizable model [33], respectively. Other simulation studies, e.g. by Powles et al. [32], also predicted the self-diffusion coefficient, achieving only a poor agreement with the experiment, cf. Fig. 11.

4.4.2. Shear viscosity

The shear viscosity of saturated liquid HCl was predicted between 160 and 300 K. Fig. 12 shows the simulation results from this work and by Kielpinski et al. [42] together with experimental data [66–68] and correlations thereof by DIPPR [56] and by Yaws [69]. Numerical data are given in Table 7 of the Supplementary material. Due to the large differences between simulation, experiment and correlations at low temperatures, the shear viscosity was additionally predicted using another simulation tool [70] employing a reverse-NEMD method [51]. EMD methods show higher statistical uncertainties than NEMD methods due to the presence of a high signal to noise ratio. As can be seen in Fig. 12, present data from EMD and NEMD methods match within their uncertainty so that it can be assumed that both simulation data sets are statistically reliable. For temperatures above 230 K, the present predictions are in good agreement with the experimental data and the DIPPR [56] correlation. However, for temperatures below 230 K, the calculated temperature dependence of the shear viscosity from simulation shows a very different inclination than the correlations, which disagree with each other. An inspection of the temperature dependence of the available experimental data shows that the data sets at high and low temperatures do not match, one of them being from the year 1906 [66]. Furthermore, for temperatures below 230 K, both correlations and the available experimental data are significantly different. Unfortunately, to our knowledge, further experimental data sets are not available and the only preceding simulation work on the prediction of the shear viscosity of HCl by Kielpinski et al. [42] based on the model by Murad et al. [37] was limited to temperatures above 250 K.

4.4.3. Thermal conductivity

Present simulation results for the thermal conductivity of saturated liquid HCl between 160 and 275 K are compared to experimental data [71] and to correlations thereof by Yaws [69] and by Kang et al. [72] in Fig. 13. Numerical results are given

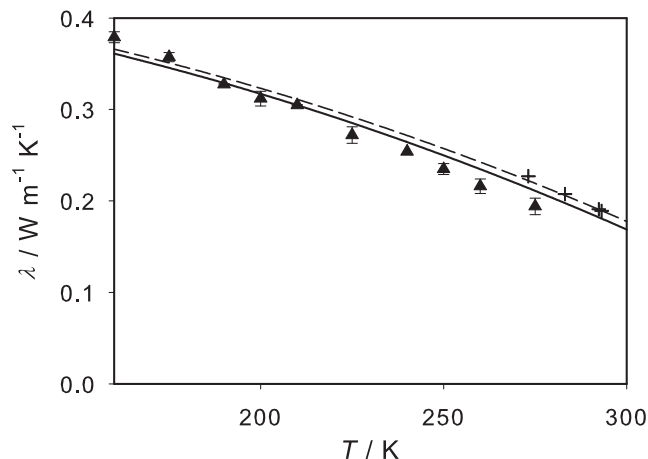


Fig. 13. Temperature dependence of the thermal conductivity of saturated liquid hydrogen chloride. Present reverse-NEMD simulation results (▲) are compared to experimental data [71] (+) and to correlations thereof by Kang et al. [72] (–) and by Yaws [69] (––).

in Table 7 of the Supplementary material. In general, a good agreement was found between simulation and both correlations, however, the simulation data tend to be lower than the correlations for temperatures above 240 K. The present results deviate on average by approximately 6% from the correlation by Yaws [69].

5. Conclusion

Self-diffusion coefficient, shear viscosity and thermal conductivity of four liquids were predicted for a wide range of thermodynamic conditions by MD simulation on the basis of rigid, non-polarizable molecular models. The self-diffusion coefficient was calculated by EMD and the Green–Kubo formalism, while the thermal conductivity was obtained using reverse boundary driven NEMD. The shear viscosity was determined by both methods. The molecular models chosen for this work are computationally inexpensive and were parameterized using experimental data on the vapor–liquid equilibrium only.

For monomethylamine, dimethylamine, dimethylether and hydrogen chloride, it was shown that molecular simulation can be used as a powerful tool for the prediction and data discrimination of transport properties over a wide range of thermodynamic conditions. In general, the predicted transport properties agree very well with the available experimental data or correlations thereof from the literature. The average deviations from experimental data are in most cases below 10%.

The results of the present work for the thermal conductivity of liquid monomethylamine along the saturation line and the shear viscosity of hydrogen chloride suggest the presence of some inaccuracies of the available experimental data and the according correlations.

List of symbols

Abbreviations

DMA	dimethylamine
DME	dimethylether
EMD	equilibrium molecular dynamics
LJ	Lennard–Jones
MMA	monomethylamine
NEMD	non-equilibrium molecular dynamics
S_i	site i

Latin symbols

A	cross sectional area
D_i	self-diffusion coefficient
J	heat flux
J_{px}	momentum flux
\mathbf{J}_p	stress tensor
k_B	Boltzmann constant
q	point charge
M	number of slabs
N	number of molecules in the ensemble
p	moment
r	site–site separation distance
t	time
T	temperature
u	interaction potential
\mathbf{v}	velocity vector
V	molar volume

Greek symbols

ϵ	Lennard–Jones energy parameter
ϵ_0	permittivity of vacuum: $\epsilon_0 = 8.8541 \times 10^{12} \text{ C}^2 \text{ J}^{-1} \text{ m}^{-1}$
η	shear viscosity
λ	thermal conductivity
μ	dipole moment
ω	orientation vector
σ	Lennard–Jones size parameter

Subscripts

a	site index
aa	related to site a –site a interactions
ab	related to site a –site b interactions
b	site index
bb	related to site b –site b interactions
c	electrostatic site index
i	related to molecule i
ij	related to molecules i and j
j	related to molecule j
k	related to molecule k
l	related to the cold slab
h	related to the hot slab

Superscripts

e	related to an electrostatic site
LJ	related to a Lennard–Jones site
x	spatial vector component in the x direction
y	spatial vector component in the y direction
z	spatial vector component in the z direction

Acknowledgements

The presented research was conducted under the auspices of the Boltzmann-Zuse Society of Computational Molecular Engineering (BZS). The simulations were performed on the national super computer NEC SX-8 at the High Performance Computing Center Stuttgart (HLRS) and on the HP X6000 super computer at the Steinbuch Center for Computing, Karlsruhe under the grant LAMO. Furthermore, the authors would like to thank Elizabeth Erazo Garzón and Emmanuel Mboo for performing numerous simulation runs.

Appendix A. Simulation details

EMD simulations were performed in two steps using the program *ms2* [73]. In the first step, a simulation in the isobaric-isothermal (NpT) ensemble was performed at the desired

temperature and pressure to obtain the density. The simulations of the saturated liquid were carried out using the corresponding saturated density of the models. The system was equilibrated over 8×10^4 time steps, followed by a production run of 5×10^5 time steps. In the second step, a canonic (NVT) ensemble simulation was performed at this temperature and density to calculate the transport properties. The simulations in the NpT and the NVT ensemble were carried out in a cubic volume with periodic boundary conditions containing 1372 molecules. Newton's equations of motion were solved using a fifth-order Gear predictor-corrector numerical integrator. The temperature was controlled by velocity scaling. In all simulations, the integration time step was 0.97 fs. The cut-off radius was set to $r_c = 15 \text{ \AA}$. Electrostatic long-range corrections were made using the reaction field technique with conducting boundary conditions ($\epsilon_{RF} = \infty$). On the basis of a center of mass cut-off scheme, the LJ long-range interactions were corrected using angle averaging [74]. The simulations were equilibrated in the NVT ensemble over 10^5 time steps, followed by production runs of 1.2 – 1.6×10^6 time steps. The self-diffusion coefficient and the shear viscosity were calculated using Eqs. (5)–(7) with up to 8000 independent time origins of the autocorrelation functions. The sampling length of the autocorrelation functions was between 8 and 12 ps, depending on the thermodynamic conditions. The separation between the time origins was chosen such that all autocorrelation functions have decayed at least to $1/e$ of their normalized value to guarantee their time independence [75]. The uncertainties of the predicted values were estimated by a block averaging method [76].

The NEMD simulations for predictions of the shear viscosity and the thermal conductivity were performed with the YASP simulation package [70]. Here, 1000 molecules were placed in a parallelepiped volume, where periodic boundary conditions were applied in all directions. The system was then equilibrated over 8×10^5 time steps at the desired temperature and pressure by NpT simulation using a weak coupling bath [77] with long-range corrections [76] for energy and pressure. The resulting density of the equilibration run was then taken to generate a new set of simulations in order to develop the thermal or shear gradient in a run over 2×10^6 time steps using the NEMD scheme. In this case, the simulation volume was divided in 20 slabs and an exchange frequency of $1/300$ (300 time steps) was used. The electrostatic long-range interactions were also treated with the reaction field technique with conducting boundary conditions. The shear viscosity and the thermal conductivity were computed via an average of six different runs. The integration of the equations of motion was performed with a time step of 1 fs and a cut-off radius of 15 \AA . A Verlet neighbor list was employed to improve the performance of the simulations.

Appendix B. Supplementary data

Supplementary data associated with this article can be found, in the online version, at [doi:10.1016/j.fluid.2011.12.009](https://doi.org/10.1016/j.fluid.2011.12.009).

References

- [1] D. Frenkel, B. Smit, *Understanding Molecular Simulation: From Algorithms to Applications*, 2nd ed., Elsevier, San Diego, 2002.
- [2] G. Guevara-Carrion, C. Nieto-Draghi, J. Vrabec, H. Hasse, *J. Phys. Chem. B* 112 (2008) 16664.
- [3] G. Guevara-Carrion, J. Vrabec, H. Hasse, *J. Chem. Phys.* 134 (2011) 074508.
- [4] G. Guevara-Carrion, J. Vrabec, H. Hasse, *Int. J. Thermophys.* submitted for publication.
- [5] F. Müller-Plathe, *J. Chem. Phys.* 106 (1997) 6082.
- [6] G.R. Maxwell, *Synthetic Nitrogen Products. A Practical Guide to the Products and Processes*, Kluwer Academic Publishers, New York, 2004.
- [7] A.B. Bauer, S. Patel, *J. Mol. Liq.* 142 (2008) 32.
- [8] T.H. Fleisch, A. Basu, M.J. Gradassi, J.G. Masin, *Stud. Surf. Sci. Catal.* 107 (1997) 117.

- [9] A.M. Arkharov, S.D. Glukhov, L.V. Grekhov, A.A. Zherdev, N.A. Ivashchenko, D.N. Kalinin, A.V. Sharaburina, A.A. Aleksandrov, *Chem. Petrol. Eng.* 39 (2003) 330.
- [10] T.A. Semelsberger, R.L. Borup, H.L. Greene, *J. Power Sources* 156 (2005) 497.
- [11] M. Sun, L. Yu, C.-Y. Sun, Y.-B. Song, J. Sun, *Fine Chem.* 11 (2003) 017.
- [12] R.L. Myers, *The 100 Most Important Chemical Compounds: A Reference Guide*, Greenwood Publishing Group, Westport, 2007.
- [13] Y.-L. Huang, M. Heilig, H. Hasse, J. Vrabec, *AIChE J.* 52 (2010) 1043.
- [14] R.C. Rizzo, W.L. Jorgensen, *J. Am. Chem. Soc.* 121 (1999) 4827.
- [15] S.O. Jónsdóttir, K. Rasmussen, *New J. Chem.* 24 (2000) 243.
- [16] Y. Boutard, P. Ungerer, J.M. Teuler, M.G. Ahunbay, S.F. Sabater, J. Pérez-Pellitero, A.D. Mackie, E. Bourrasseau, *Fluid Phase Equilib.* 236 (2005) 25.
- [17] C.D. Wick, J.M. Stubbs, N. Rai, J.I. Siepmann, *J. Phys. Chem. B* 109 (2005) 18974.
- [18] F.S. Baskaya, N.H. Gray, Z.N. Gereks, J.R. Elliott, *Fluid Phase Equilib.* 236 (2005) 42.
- [19] E.M. Cabaleiro-Lago, M.A. Ríos, *J. Chem. Phys.* 113 (2000) 9523.
- [20] T. Kosztolányi, I. Bakó, G. Pálkás, *J. Chem. Phys.* 118 (2003) 4546.
- [21] P.G. Kusalik, D. Bergman, A. Laaksonen, *J. Chem. Phys.* 113 (2000) 8036.
- [22] R.W. Impey, M. Sprik, M.L. Klein, *J. Am. Chem. Soc.* 109 (1984) 5900.
- [23] H. Feng, X. Liu, W. Gao, X. Chen, J. Wang, L. Chen, H.-D. Lüdemann, *Phys. Chem. Chem. Phys.* 12 (2010) 15007.
- [24] J.M. Briggs, T. Matsui, W.L. Jorgensen, *J. Comput. Chem.* 11 (1990) 958.
- [25] W.L. Jorgensen, D.S. Maxwell, J. Tirado-Rives, *J. Am. Chem. Soc.* 118 (1996) 11225.
- [26] J.M. Stubbs, J.J. Potoff, J.I. Siepmann, *J. Phys. Chem. B* 108 (2004) 17596.
- [27] O. Unlu, N.H. Gray, Z.N. Gereks, J.R. Elliott, *Ind. Eng. Chem. Res.* 43 (2004) 1788.
- [28] J.N. Hermida-Ramón, M.A. Ríos, *Chem. Phys.* 262 (2000) 423.
- [29] B. Lin, J.W. Halley, *J. Comput. Chem.* 99 (1995) 16474.
- [30] T.R. Pollock, P. Crozier, R.L. Rowley, *Fluid Phase Equilib.* 217 (2004) 89.
- [31] M.B.H. Ketko, J.J. Potoff, *Mol. Simul.* 33 (2007) 769.
- [32] J.G. Powles, W.A.B. Evans, E. McGrath, K.E. Gubbins, S. Murad, *Mol. Phys.* 38 (1979) 893.
- [33] S. Murad, K.E. Gubbins, J.G. Powles, *Mol. Phys.* 43 (1980) 253.
- [34] I.R. McDonald, S.F. O'Shea, D.G. Bounds, M.L. Klein, *J. Chem. Phys.* 72 (1980) 5710.
- [35] M.L. Klein, I.R. McDonald, *Mol. Phys.* 42 (1981) 243.
- [36] C. Votava, R. Ahlrichs, A. Geiger, *J. Chem. Phys.* 78 (1983) 6841.
- [37] S. Murad, A. Papaioannou, J.G. Powles, *Mol. Phys.* 56 (1985) 431.
- [38] D. Gutwerk, T. Bausenwein, H. Bertagnolli, *Ber. Bunsenges. Phys. Chem.* 98 (1994) 920.
- [39] C. Martin, E. Lomba, M. Lombardo, F. Lado, J.S. Hoye, *J. Chem. Phys.* 100 (1994) 1599.
- [40] T. Yogi, *J. Phys. Soc. Jpn.* 66 (1997) 641.
- [41] V. Dubois, A. Pasquarello, *J. Chem. Phys.* 122 (2005) 114512.
- [42] A.L. Kielbinski, K. Mansour, S. Murad, *Int. J. Thermophys.* 7 (1986) 421.
- [43] T. Schnabel, J. Vrabec, H. Hasse, *Fluid Phase Equilib.* 263 (2008) 144.
- [44] B. Eckl, J. Vrabec, H. Hasse, *J. Phys. Chem. B* 112 (2008) 12710.
- [45] J.O. Hirschfelder, C.F. Curtiss, R.B. Bird, *Molecular Theory of Gases and Liquids*, John Wiley & Sons, New York, 1954.
- [46] M.S. Green, *J. Chem. Phys.* 22 (1954) 398.
- [47] R. Kubo, *J. Phys. Soc. Jpn.* 12 (1957) 570.
- [48] K.E. Gubbins, *Statistical Mechanics*, vol. 1, The Chemical Society Burlington House, London, 1972.
- [49] C. Hoheisel, *Phys. Rep.* 245 (1994) 111.
- [50] P. Bordat, F. Müller-Plathe, *J. Chem. Phys.* 116 (2002) 3362.
- [51] F. Müller-Plathe, P. Bordat, *Lect. Notes Phys.* 640 (2004) 310.
- [52] L. Chen, T. Groß, H.-D. Lüdemann, *Phys. Chem. Chem. Phys.* 1 (1999) 3503.
- [53] N.P. Isakova, L.A. Oshueva, *Zh. Prikl. Khim.* 41 (1968) 2805.
- [54] R.C. Makhija, R.A. Stairs, *Can. J. Chem.* 48 (1970) 1214.
- [55] R.A. Stairs, *J. Chem. Eng. Data* 25 (1980) 379.
- [56] R.L. Rowley, W.V. Wilding, J.L. Oscarson, Y. Yang, N.F. Giles, DIPPR: Data Compilation of Pure Chemical Properties, Design Institute for Physical Properties, AIChE, New York, 2010.
- [57] *Thermal Conductivity of Liquid Aliphatic Amines*, Report No.: ESDU-78022, Engineering Sciences Data Unit International Ltd., London, 1978.
- [58] R.W. Gallant, *Physical Properties of Hydrocarbons*, Gulf Publishing Co., Houston, 1968–1970.
- [59] V.A. Fedosov, *Teplofiz. Vys. Temp.* 18 (1980) 1324.
- [60] E.W. Washburn, *International Critical Tables of Numerical Data, Physics, Chemistry, and Technology*, McGraw-Hill, New York, 1926–1933.
- [61] W. Braker, A.L. Mossman, *The Matheson Unabridged Gas Data Book*, Matheson Gas Products, East Rutherford, NJ, 1974.
- [62] A. Heinrichschramm, A. Price, H.-D. Lüdemann, *Z. Naturforsch. A* 50 (1995) 145.
- [63] M.L. Huber, A. Laesecke, R.A. Perkins, *Ind. Eng. Chem. Res.* 42 (2003) 3163.
- [64] D.E. O'Reilly, *J. Chem. Phys.* 49 (1968) 5416.
- [65] K. Krynicki, S.N. Changdar, J.G. Powles, *Mol. Phys.* 39 (1980) 773.
- [66] B.D. Steele, D. McIntosh, E.H. Archibald, *Philos. Trans. R. Soc. Lond. A* 205 (1906) 99.
- [67] K. Krynicki, J.W. Hennel, *Acta Phys. Pol.* 24 (1963) 269.
- [68] J. D'Ans, J. Bartels, P. ten Bruggencate, A. Eucken, G. Joos, W.A. Roth (Eds.), *Landolt-Börnstein: Zahlenwerte und Funktionen aus Physik, Chemie, Astronomie, Geophysik und Technik*, 5. Teil, Bandteil a: Transportphänomene I, Springer Verlag, Berlin, 1969.
- [69] C.L. Yaws, *Physical Properties*, McGraw-Hill, New York, 1977.
- [70] F. Müller-Plathe, *Comput. Phys. Commun.* 78 (1993) 77.
- [71] D.T. Jamieson, J.B. Irving, J.S. Tudhope, *Liquid Thermal Conductivity a Data Survey to 1973*, Her Majesty's Stationery Office, Edinburgh, 1975.
- [72] J.W. Kang, K.-P. Yoo, H.Y. Kim, H. Lee, D.R. Yang, C.S. Lee, *Int. J. Thermophys.* 22 (2001) 487.
- [73] S. Deublein, B. Eckl, J. Stoll, S.V. Lishchuk, G. Guevara-Carrion, C.W. Glass, T. Merker, M. Bernreuther, J. Vrabec, H. Hasse, *Comput. Phys. Commun.* (2011), doi:10.1016/j.cpc.2011.04.026.
- [74] R. Lustig, *Mol. Phys.* 65 (1988) 175.
- [75] M. Schoen, C. Hoheisel, *Mol. Phys.* 52 (1984) 33.
- [76] M.P. Allen, D.J. Tildesley, *Computer Simulation of Liquids*, 2nd ed., Clarendon, Oxford, 1987.
- [77] H.J.C. Berendsen, J.P.M. Postma, W.F. van Gunsteren, A. Di Nola, J.R. Haak, *J. Chem. Phys.* 81 (1984) 3684.